Mon. Not. R. Astron. Soc. **413,** 852–862 (2011) doi:10.1111/j.1365-2966.2010.18173.x

The radio–γ-ray connection in *Fermi* blazars

G. Ghirlanda,★ G. Ghisellini, F. Tavecchio, L. Foschini and G. Bonnoli
INAF – Osservatorio Astronomico di Brera, Via Bianchi 46, I-23807 Merate, Italy

Accepted 2010 December 8. Received 2010 December 8; in original form 2010 July 15

ABSTRACT

We study the correlation between the γ-ray flux (F_γ), averaged over the first 11 months of the *Fermi* survey and integrated above 100 MeV, and the radio flux density ($F_{\rm r}$ at 20 GHz) of *Fermi* sources associated with a radio counterpart in the 20-GHz Australia Telescope Compact Array (AT20G) survey. Considering the blazars detected in both bands, the correlation is highly significant and has the form $F_\gamma \propto F_{\rm r}^{0.85\pm0.04}$, similar to BL Lacertae objects and flat-spectrum radio quasars. However, only a small fraction ($\sim$1/15) of the AT20G radio sources with flat radio spectra are detected by *Fermi*. To understand if this correlation is real, we examine the selection effects introduced by the flux limits of both the radio and the γ-ray surveys, and the importance of variability of the γ-ray flux. After accounting for these effects, we find that the radio–γ-ray flux correlation is real, but its slope is steeper than the observed one, that is, $F_\gamma \propto F_{\rm r}^{\delta}$ with δ in the range 1.25–1.5. The observed F_γ–$F_{\rm r}$ correlation and the fraction of radio sources detected by *Fermi* are reproduced assuming a long-term γ-ray flux variability, following a lognormal probability distribution with standard deviation $\sigma \geq 0.5$ (corresponding to F_γ varying by at least a factor of 3). Such a variability is compatible, even if not necessarily equal, with what is observed when comparing, for the sources in common, the EGRET and the *Fermi* γ-ray fluxes (even if the *Fermi* fluxes are averaged over $\sim$1 yr). Another indication of variability is the non-detection of 12 out of 66 EGRET blazars by *Fermi*, despite its higher sensitivity. We also study the strong linear correlation between the γ-ray and the radio luminosity of the 144 AT20G–*Fermi* associations with known redshift and show, through partial correlation analysis, that it is statistically robust. Two possible implications of these correlations are discussed: the contribution of blazars to the extragalactic γ-ray background and the prediction of blazars that might undergo extremely high states of γ-ray emission in the next few years.

Key words: radiation mechanisms: non-thermal – BL Lacertae objects: general – quasars: general – radio continuum: general – X-rays: general.

1 INTRODUCTION

The Large Area Telescope (LAT) onboard the *Fermi* satellite (Atwood et al. 2009) detected 1451 sources [Fermi Large Area Telescope First Source Catalog (1FGL)] in the γ-ray band above 100 MeV with a significance $\geq 4.5\sigma$ during its first 11-month survey (Abdo et al. 2010h): 831 out of 1451 are classified as active galactic nuclei (AGNs) (Abdo et al. 2010a).[1]

We cross-correlated (Ghirlanda et al. 2010, hereinafter G10) the *Fermi* 1FGL with a complete flux-limited sample of radio sources detected by the Australia Telescope Compact Array (ATCA) in a survey conducted at 20 GHz with a flux density limit $\geq$40 mJy (Murphy et al. 2010). The cross-correlation led to the identification of highly probable (association probability >80 per cent) radio counterparts for 230 1FGL sources (hereinafter the 1FGL–AT20G associations, where AT20G represents the 20-GHz Australia Telescope Compact Array) (see also Mahony et al. 2010). 222 of these are already classified in the First LAT AGN Catalog (1LAC, Abdo et al. 2010a) as BL Lacertae (BL Lac) objects (54), flat-spectrum radio quasars (FSRQs) (112), candidate blazars of unknown class (46) or other type of AGNs (10). Among the generic class of 'AGNs', there are different source types: starburst galaxies (NGC 253, M82: Abdo et al. 2010b), starburst/Seyfert 2 (NGC 4945, Lenc & Tingay 2009), a low-excitation Fanaroff–Riley type I (FR I) radio galaxy (PKS 0625–35, Gliozzi et al. 2008), a high-excitation FR I radio galaxy (Cen A, Abdo et al. 2010f,g) and a narrow-line Seyfert 1 (PKS 2004−447, Abdo et al. 2009b). The cross-correlation of G10 also led to the discovery of eight new associations among which two are classified as FSRQs and one as BL Lac. *Therefore, most of the 1FGL–AT20G associations are blazars of the FSRQ or BL Lac classes.*

★E-mail: giancarlo.ghirlanda@brera.inaf.it
[1] http://heasarc.gsfc.nasa.gov/W3Browse/fermi/fermilac.html

The 230 1FGL–AT20G associations also have typically flat radio spectra with spectral index in the range $-0.5 < \alpha_{(5\text{-}20\,\mathrm{GHz})} < 0.5$ and centred at $\alpha_{(5\text{-}20\,\mathrm{GHz})} \sim 0$ (with $F_\nu \propto \nu^\alpha$). However, the radio AT20G sources associated with a *Fermi* source of the 1FGL are only a minor fraction ($\sim$1/15) of more than 3600 AT20G sources with flat radio spectra [i.e. $\alpha_{(5\text{-}20\,\mathrm{GHz})} > -0.5$].

The 230 1FGL–AT20G associations show a statistically significant correlation between the γ-ray flux and the 20-GHz flux density: $F_\gamma \propto F_\mathrm{r}^{0.85\pm0.04}$ (see G10). This correlation has a similar slope when considering BL Lac objects and FSRQs separately.

The relevance of the F_γ–F_r correlation is two-fold: it can help to estimate the contribution of blazars to the γ-ray background (e.g. Stecker, Salamon & Malkan 1993) and it could shed light on the physical link between the emission processes in the radio and γ-ray energy bands. Indeed, the so-called 'blazar sequence' (Fossati et al. 1998; Ghisellini et al. 1998) was built by dividing blazars into bins of radio luminosity, thought to be a proxy for the bolometric one, and establishes a link between the radio and the γ-ray emission. On the other hand, the radio- and γ-ray-emitting regions are probably different, since the rapid variability in the γ-ray flux suggests a compact size (see e.g. Tavecchio et al. 2010), for which the synchrotron spectrum is self-absorbed up to hundreds of GHz. We therefore believe that the link between the radio and the γ-ray emission (if any) must be indirect. One possibility is that both track the jet power, with the radio averaging it on a larger time-scale than the γ-ray emission.

The radio–γ-ray properties of EGRET blazars suggested the possible existence of a F_γ–F_r correlation considering bright γ-ray sources (Taylor et al. 2007), although at low radio fluxes, no conclusive claim could be made (e.g. Mucke et al. 1997). A possible correlation of F_γ with the radio flux at 8.4 GHz was found in the population of blazars detected by *Fermi* in its first 3-month survey [Fermi LAT Bright AGN Sample (LBAS), Abdo et al. 2009a]. This correlation was more significant for BL Lac objects (chance probability $P = 0.05$ per cent) than for FSRQs ($P = 8$ per cent). An updated version of the F_γ–F_r correlation, based on the *Fermi* 1LAC, is reported by Giroletti et al. (2010). Recent studies of the radio–γ flux correlation in the LBAS sources (Kovalev 2009; Kovalev et al. 2009) were conducted using the MOJAVE sample of extragalactic sources (with a flux limit of 1.5 Jy at 15 GHz). Kovalev (2009) finds that the parsec-scale radio emission and the γ-ray flux are strongly related in bright γ-ray objects, suggesting that *Fermi* selects the brightest objects from a flux-density-limited sample of radio-loud sources.

The F_γ–F_r correlation is subject to the biases related to the flux limits of the radio and γ-ray surveys. However, these biases acting on the radio and the γ-ray surveys are independent. The AT20G–1LAC associations have been found by cross-correlating two independent surveys: the radio AT20G (Murphy et al. 2010) and the *Fermi* 11-month survey catalogue (Abdo et al. 2010h).

The two main problems we want to tackle in this paper are (1) to understand why only a minor fraction ($\sim$1/15) of radio sources (of the AT20G survey) are detected in γ-rays by *Fermi*, despite the possible existence of a correlation between the radio and the γ-ray flux; and (2) to recover the true radio–γ-ray flux correlation by accounting for the selection effects of both the radio and the *Fermi* survey.

An important aspect which could have impact on these issues is the γ-ray variability of blazars. We will consider in this paper two possible variability patterns: a long-term variability which is observed, for instance, when comparing the fluxes measured by EGRET and by *Fermi* (almost 10 years later) for the sources in common, and a short-term variability observed so far on daily time-scales in the brightest sources.

This paper is organized as follows. In Section 2, the correlation between the γ-ray and the radio flux of the AT20G–*Fermi* associations is presented and in Section 3, the duty cycle of blazars in the γ-ray band is discussed. In Section 4, we describe the method used to reconstruct the true γ-ray–radio flux correlation and in Section 5, we show our results and discuss their main possible implications. A summary and conclusions are given in Section 6.

2 THE OBSERVED RADIO–γ-RAY CORRELATION

Fig. 1 shows the correlation found by G10 with the 230 1FGL *Fermi* sources associated with a radio counterpart in the AT20G sample (squares in Fig. 1). For these associations, we computed the *Fermi* flux by integrating their spectrum (reported in the 1FGL) above 100 MeV. The best fit (computed with the bisector method) of the F_γ–F_r correlation is $F_\gamma \propto F_\mathrm{r}^{0.8\pm0.04}$. In the following, we will refer to the latter as the 'observed correlation' F_γ–F_r. Our aim is to account for the possible selection effects acting on the F_γ–F_r plane and recover the 'real correlation' $\hat{F}_\gamma$–$\hat{F}_\mathrm{r}$ which can have a different slope and normalization with respect to the observed one. With the 'hat' quantities, we indicate the γ-ray and radio flux of the sources generated through the simulations described in Section 4. To these sources we apply the selection effects in order to reproduce the observed correlation F_γ–F_r. In the simulations (see Section 4), we consider the real radio sources by adopting their real radio fluxes (reported in the AT20G survey). Therefore, F_r and $\hat{F}_\mathrm{r}$ coincide, whereas for each real radio source, the $\hat{F}_\gamma$ is that obtained by assuming a certain γ-ray variability (described in Section 3).

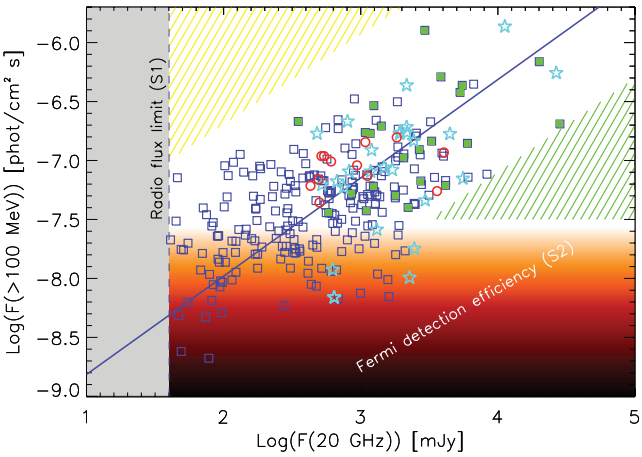

Figure 1. The F_γ–F_r correlation found with the 1FGL sources with a counterpart in the 20-GHz radio survey AT20G catalogue (open squares). The solid line is the fitting correlation (with slope $\sim$0.8). Also shown are the two main selection effects that we consider in this paper (see text): the radio flux limit (S1) at 40 mJy represented by the grey vertical shaded region and the *Fermi* detection sensitivity which increases for increasing γ-ray fluxes and is represented by the bottom shaded region. The two hatched triangles represent the region of the plane where we should expect to find sources if there is no F_γ–F_r correlation. The absence of sources in these triangular regions is an indication of the existence of such a F_γ–F_r correlation. The 3EG sources (Hartman et al. 1999) also detected by *Fermi* and not present in the AT20G survey (because at Dec. $> 0^\circ$) are shown with open (cyan) stars, those present in the AT20G survey are shown by filled (green) squares and the 12 3EG sources not detected by *Fermi* are shown with (red) open circles.

The two main selection effects that could bias the F_γ–F_r correlation are the flux limit of the AT20G survey $F_r > 40$ mJy (S1) and the *Fermi* detection efficiency in the 0.1–100 GeV energy band (S2). These are schematically shown in Fig. 1. While the AT20G radio survey has a well-defined 20 GHz flux limit (shaded grey region in Fig. 1), the *Fermi* sensitivity depends on several parameters (Abdo et al. 2010c) like the source spectrum in the GeV band and its position in the sky where the different intensity and anisotropy of the Galactic and extragalactic γ-ray backgrounds can limit the detection efficiency as a function of the source flux. For instance, simulations of sources distributed at high Galactic latitudes $|b| > 20^\circ$ show that the detection efficiency is only 1 per cent for sources with $F_\gamma \sim 10^{-8}$ photon cm^{-2} s^{-1}, although such a flux is above the lowest flux measured by *Fermi* (Abdo et al. 2010c). This is due to the combination of two main effects: the intensity of the local background and the source spectral index (see Abdo et al. 2010c for details). We show in Fig. 1 the *Fermi* detection efficiency as a shaded coloured region. This is obtained from the efficiency curve reported in fig. 7 of Abdo et al. (2010c) that assumes a distribution of γ-ray photon spectral indices centred at $\Gamma = 2.4$ and with a dispersion of 0.28.

Considering the distribution of sources in Fig. 1, and the two instrumental selection effects S1 and S2, we note that there are two regions in the F_γ–F_r plane (the hatched regions in Fig. 1) where there are no sources. Although source number counts decrease with increasing fluxes (both in the radio and in the γ-ray band), there seems to be no apparent instrumental selection effect preventing the detection of bright γ-ray sources with intermediate/low radio fluxes (in the yellow-hatched upper left-hand triangle) as well as bright radio sources above the *Fermi* detection limit (in the green-hatched lower right-hand triangle). This suggests that the observed correlation is true, although we expect that its real slope and normalization can be different from those derived from the observed sources in the F_γ–F_r plane, because the latter is strongly biased at low F_γ and F_r by the instrumental selections effects S1 and S2 (as shown in Fig. 1).

3 THE DUTY CYCLE OF THE γ-RAY FLUX IN BLAZARS

The variability of the γ-ray emission in blazars has long since been discussed in the literature. It is now with *Fermi* that robust claims can be made, thanks to an almost continuous monitoring of the γ-ray sources in the sky with a relatively high sensitivity which allows to probe the variations in the flux both on long time-scales (increasing with the mission elapsed time) and on short time-scales (from months down to days for the brightest sources).

Variability of the γ-ray flux of blazars could be the key ingredient to explain why only a minor fraction of the radio sources detected in the AT20G survey have been detected by *Fermi* in the γ-ray band and it could help to reconstruct the true $\hat{F}_\gamma$–$\hat{F}_r$ correlation accounting for the *Fermi* detection selection effect.

In the following, we will refer to two main variability patterns of the γ-ray flux of blazars: (1) a long-term variability which seems to follow a lognormal probability distribution with $\sigma \sim 0.5$; and (2) a short-term variability which follows a non-symmetric probability distribution skewed towards low flux levels.

3.1 Long-time-scale variability

In the Third EGRET Catalog (3EG, Hartman et al. 1999), there are 66 high-confidence AGNs. 54 of these are detected by *Fermi*, while 12 are not present in the 1LAC. Among the 54 3EG sources detected by *Fermi*, 48 have a published radio flux density at ∼20 GHz. Those in the Northern hemisphere and those in the Southern hemisphere (already present in the 1LAC–AT20G associations) are highlighted in Fig. 1 (shown by open cyan stars and filled green squares, respectively).

The 48 3EG sources (out of the 54 detected by *Fermi*), for which we could find the radio flux density (Fig. 1), are consistent with the F_γ–F_r correlation found through the 1FGL–AT20G associations.

The 12 3EG sources (classified as blazars in Hartman et al. 1999) not detected by *Fermi* in its 11-month survey are shown in Fig. 1 using their 3EG γ-ray flux (open red circles).

The EGRET flux of these 12 sources is above the *Fermi* detection sensitivity (shown by the shaded region in Fig. 1). They occupy a region where no apparent instrumental selection effect is present. Therefore, the non-detection of these 3EG sources by *Fermi* must be due to their γ-ray variability over about a decade.

It is interesting to compare the γ-ray flux of the sources detected both by EGRET and by *Fermi* (about 10 years after). When doing this, we must recall that the *Fermi* fluxes are averages over the 11 months of the survey, while the EGRET fluxes correspond to averages over a shorter time-interval, typically few months, since they are derived from pointed observations.

Fig. 2 shows the 3EG fluxes and those measured by *Fermi* for the common sources. We also show in Fig. 2 the 12 3EG sources not detected by *Fermi* as upper limits (green arrows in the top panel) and as lower limits on the EGRET-to-*Fermi* flux ratio (arrows in the bottom panel), obtained assuming, for *Fermi*, a limiting flux of 2.5×10^{-8} photon cm^{-2} s^{-1}, that is, corresponding to the upper boundary of the shaded region S2 shown in Fig. 1. On average (see the bottom panel of Fig. 2), the EGRET fluxes were larger than those of *Fermi*. We find that the ratio of the flux measured by EGRET and by *Fermi* is distributed as a lognormal with standard deviation $\sigma = 0.5$ (bottom panel of Fig. 2). We note that this distribution also fully comprises the lower limits of the 12 3EG sources not detected by *Fermi*. However, given the presence of these lower limits in the bottom panel of Fig. 2, we also tested in our simulations a lognormal variability with $\sigma = 0.78$ (represented in Fig. 2 by the dashed grey line), that is, corresponding to a variation in the flux by a factor of ∼6.

If this is representative of a *decadal flux variability* of these sources, then it explains why a fraction of EGRET sources were not detected by *Fermi*, despite its better sensitivity.

This result, that is, the possibility that the GeV flux of γ-ray blazars (even if time-averaged over ∼1 yr) can vary by a factor of 3 (at 1σ) over ∼10 yr will be used in the next section to reconstruct the true $\hat{F}_\gamma$–$\hat{F}_r$ correlation by accounting for the selection effect S2.

3.2 Short-time-scale variability

Tavecchio et al. (2010) (see also Foschini et al. 2010) studied the variability of the GeV flux in the two blazars 3C 454.3 (see also Bonnoli et al. 2011) and PKS 1510–089 detected by *Fermi* and found variability on few days time-scale by considering their emission as observed by *Fermi* in 1 year. During exceptionally bright events, significant variability was also found on intraday time-scales (Abdo et al. 2010e; Tavecchio et al. 2010). Tavecchio et al. (2010) also found that, in these two sources, the differential flux curve (representing the number of days a source spends at a given flux level F_γ) has a similar pattern (also present in other sources, Tavecchio et al., in preparation) with a rising power law and a faster decay (steep

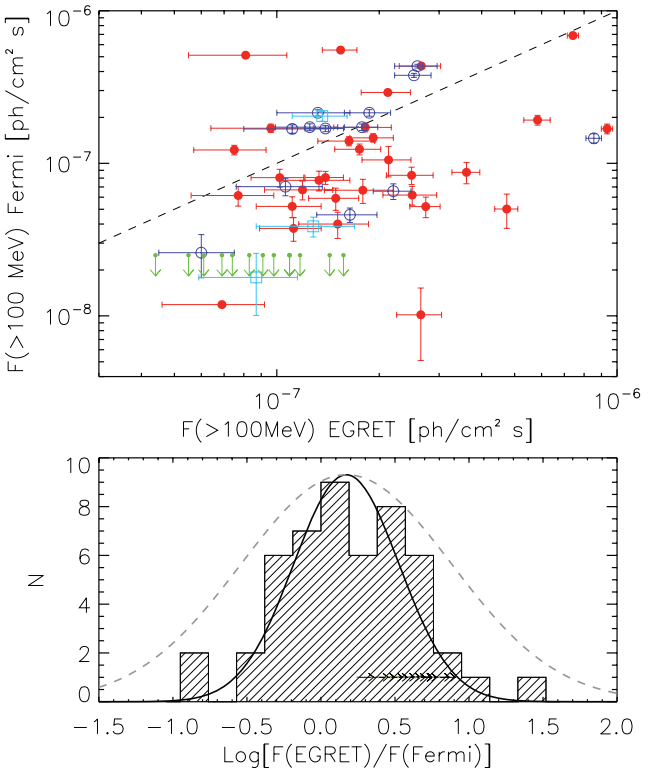

Figure 2. Top panel: comparison of *Fermi* and 3EG fluxes (>100 MeV) of the 48 3EG sources detected by *Fermi* (reported in the 1LAC sample) and for which we could find a radio flux density at ∼20 GHz in the literature. The 12 3EG sources not detected by *Fermi* are shown as upper limits (green arrows). FSRQs, BL Lac objects and sources classified as 'AGNs' in the 1LAC are shown with different symbols (filled circles, open circles and open squares, respectively). The dashed line represents equality. Bottom panel: distribution of the ratio between the flux measured by EGRET and by *Fermi* for the sources in common. The 12 3EG sources not detected by *Fermi* are represented as lower limits (arrows). The hatched distribution can be represented by a Gaussian function (solid line) with central value $\mu = 0.17$ and standard deviation $\sigma = 0.5$. It is also shown a Gaussian (dotted grey line) with $\sigma = 0.78$, that is, a factor of 2 larger in linear scale, which is tested in the simulations (see Section 5).

power law), bracketing a characteristic peak. This short-time-scale variability can be described as

$$N(F_\gamma) \propto \frac{(F_\gamma/F_{\gamma,\rm break})^a \exp(-F_\gamma/F_{\rm cut})}{1+(F_\gamma/F_{\gamma,\rm break})^{b+a}}, \quad (1)$$

where $F_{\gamma,\rm break}$ is the flux corresponding to the break between the low-flux power law with slope a and the high-flux power law with slope b, and $F_{\rm cut}$ is the flux of the exponential cut-off. Since we are concerned with γ-ray fluxes *averaged* over 1 yr, the short-time-scale variability can produce *very modest* variations in the averaged flux.

Instead, the long-time-scale variability observed in the common EGRET/*Fermi* sources can change the flux by a factor of 3 (at 1σ level), implying a larger spread of the γ-ray flux, although corresponding to longer time-scales.

4 THE SIMULATION

We want to constrain the normalization and slope of the real $\hat{F}_\gamma$–$\hat{F}_{\rm r}$ correlation that reproduces the observed distribution of the 230 1LAC–AT20G associations shown by squares in Fig. 1 and, at the same time, accounts for the non-detection of the large majority of the radio sources of the AT20G sample. Even if the γ-ray-detection rate approaches 100 per cent at the largest radio fluxes and decreases for lower radio fluxes, this is not a trivial task. This is because there are many radio sources, undetected by *Fermi*, with a radio flux comparable or even larger than those that are instead detected in γ-rays.

By accounting for the *Fermi* detection efficiency and for the assumed duty cycle of blazars in the γ-ray band, we search for the $\hat{F}_\gamma$–$\hat{F}_{\rm r}$ correlation that produces a distribution of simulated sources in the F_γ–$F_{\rm r}$ plane which matches the observed one.

In particular, we consider all the radio sources with flat radio spectrum in the AT20G survey and assign to them a γ-ray flux according to a given $\hat{F}_\gamma$–$\hat{F}_{\rm r}$ correlation (whose normalization and slope are the free parameters that we want to constrain). Then we shuffle the γ-ray flux of each source according to a law which is representative of the γ-ray variability and apply the *Fermi* detection sensitivity to identify those simulated sources that should be detected by *Fermi*. In this way, we populate the F_γ–$F_{\rm r}$ plane with simulated sources observable by *Fermi* for any assumed $\hat{F}_\gamma$–$\hat{F}_{\rm r}$ correlation. We constrain the slope and normalization of the $\hat{F}_\gamma$–$\hat{F}_{\rm r}$ correlation by requiring that (i) the number of sources that should be detected by *Fermi* is consistent with the real number of sources defining the F_γ–$F_{\rm r}$ correlation (i.e. 230 ± 15); and (ii) the distribution of $F_{\rm r}$ and F_γ of the simulated sources is consistent with those of the real sources (this is evaluated through the Kolmogorov–Smirnov (KS) test, performed separately, between the $F_{\rm r}$ and F_γ distributions of the simulated and real sources). The details of the simulation and its assumptions are described below and we present our results in Section 5.

The simulation relies on some input assumptions.

(i) The true $\hat{F}_\gamma$–$\hat{F}_{\rm r}$ correlation is modelled as a power law

$$\log(\hat{F}_\gamma) = \hat{K} + \hat{\delta}\log(\hat{F}_{\rm r}), \quad (2)$$

where the normalization $\hat{K}$ and the slope $\hat{\delta}$ are the free parameters that we aim to constrain. The normalization is computed at 150 mJy in our simulations. This particular value corresponds to the average of the radio fluxes of the AT20G sources with flat radio spectrum used for the simulations.

(ii) We consider the 3686 radio sources of the AT20G survey with flat radio spectrum, that is, $\alpha_{(5\text{-}20\,\rm GHz)} > -0.5$, similar to the radio spectrum of the 230 1FGL–AT20G associations defining the observed F_γ–$F_{\rm r}$ correlation.

(iii) The γ-ray flux variability: we assign to each radio source with a certain $\hat{F}_\gamma$ (given by equation 2) a flux F_γ according to one of the two possible variability functions described in Section 3. First, we assume the short-time-scale variability function, described by equation (1). Since we are concerned with averaged (over 11 months) fluxes, we extract 11 γ-ray fluxes from the $N(F)$ distribution of equation (2) after having fixed its parameters to $F_{\gamma,\rm break} = \hat{F}_\gamma$ and always setting $a = 1.5$, $b = 3$ and $F_{\rm cut} = 5F_{\gamma,\rm break}$. We then average the 11 values of F_γ obtained in this way for each simulated source. The obtained flux is different from initial $\hat{F}_\gamma$, but by a small factor, and we anticipate that the dispersion induced by this treatment of variability is much smaller than the dispersion of the real sources in the F_γ–$F_{\rm r}$ plane along the F_γ axis.

For this reason we adopted, as a second choice, the long-term variability function, that is, a lognormal distribution with assigned standard deviation. This assumption is motivated by the comparison of the EGRET and *Fermi* flux for the common sources shown in Fig. 2 (see Section 3). The bottom panel of Fig. 2 shows that the

distribution of the flux ratio has a standard deviation of 0.5 which we also assume in our simulation. However, we will test a lognormal variability function with larger/lower standard deviation.

We stress that while the variability function of equation (1) is representative of the blazar activity over 1 yr, the lognormal with $\sigma = 0.5$ found in Section 3 corresponds to a variability over 10 yr at least, that is, the time between the EGRET and *Fermi* measurement of the *average* flux of the sources in common. Furthermore, it is already indicative of how the $\sim$1 yr *average* γ-ray flux varies, not of the variations occurring on shorter time-scales, as, instead indicated by equation (1). For this reason, we will extract only one flux from this lognormal variability distribution.

We did not model the possible radio variability of blazars. This is motivated by the fact that we simulate the γ-ray flux of real radio sources, that is, those with flat radio spectra in the AT20G complete survey. These are 3686 sources with $F_{\rm r} \geq 40$ mJy: their large number ensures that we are sampling the possible range of variability of the radio flux density.

4.1 One illustrative example

In Fig. 3, we show an example of a simulation. For this example, we have assumed a $\hat{F}_\gamma$–$\hat{F}_{\rm r}$ correlation with slope $\hat{\delta} = 1.3$ and $\hat{K} = -8.6$ at 150 mJy. After having assigned to each radio source its corresponding $\hat{F}_\gamma$, we have extracted its F_γ from a lognormal distribution peaking at $\hat{F}_\gamma$ and having a dispersion $\sigma = 0.5$. The sources simulated in this way are shown by the grey dots in Fig. 3 and the assumed $\hat{F}_\gamma$–$\hat{F}_{\rm r}$ correlation is shown by the triple-dot–dashed (green) line. Then we selected the sources detectable by *Fermi* (red dots) with the following procedure. We have considered the *Fermi* γ-ray-detection efficiency (selection effect S2) which is a function of the γ-ray flux (shaded area in Fig. 1). For S2 we used the detection efficiency curve presented in fig. 7 of Abdo et al. (2010c) which was obtained through simulations of sources at Galactic latitudes $|b| > 20^\circ$.

For sources at low Galactic latitudes, the level of the Galactic background and the larger number of sources may reduce the detection efficiency. Therefore, we mimic this effect by considering a detection efficiency reduced by a factor of 3 for sources at $-20^\circ < b < 20^\circ$. This choice is motivated by Fig. 4 where we show the γ-ray flux distribution of the *Fermi* sources of the 1LAC sample located at high Galactic latitudes ($|b| > 20^\circ$, solid histogram) and located along the Galactic plane ($|b| < 20^\circ$, dotted blue histogram). The two curves matching the left-hand side of the histograms represent the detection efficiency rescaled by a factor of 3 for the sources at low Galactic latitudes.

Among the simulated sources in a given bin of γ-ray flux, we randomly extract a fraction of sources corresponding to the *Fermi* detection efficiency (from Abdo et al. 2010c) in that flux bin. This corresponds to the application of the S2 selection bias. The

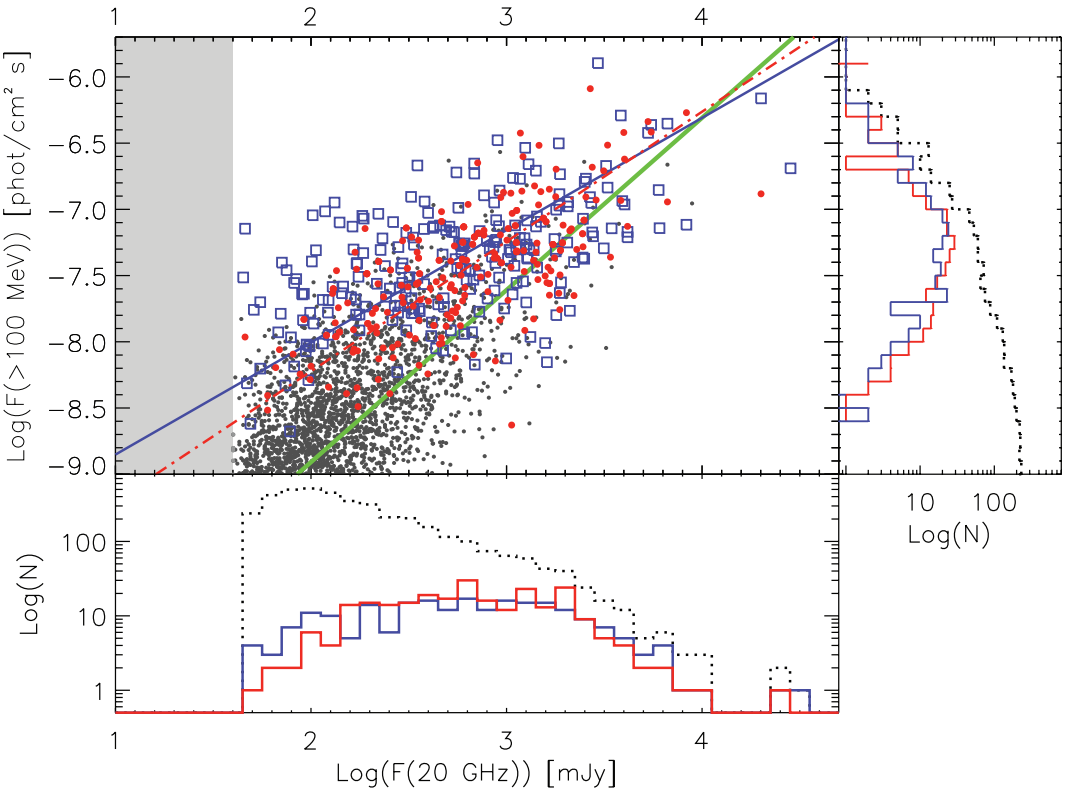

Figure 3. Example of a simulation of sources following the true correlation $\hat{F}_\gamma$–$\hat{F}_{\rm r}$ (triple dot–dashed green line) with $\hat{\delta} = 1.3$ and obtained with a γ-ray lognormal variability distribution with $\sigma_\gamma = 0.5$. Filled black dots are the real AT20G sources with flat radio spectra [$\alpha_{(5-20\,{\rm GHz})} > -0.5$] simulated with the lognormal F_γ variability function. The red points are 250 simulated sources which can be detected by *Fermi* according to its detection efficiency curve (selection effect S2, Abdo et al. 2010c). The dot–dashed line is the best-fitting correlation of simulated sources and the solid blue line is the best fit to the real sources. The open blue squares are the 230 real sources of G10. The bottom and right-hand-side panels show the $F_{\rm r}$ and F_γ distributions of the total simulated sample (dotted black line) and of the simulated sources after the application of the selection effects (red line). The distribution of the fluxes of the real sources detected by *Fermi* is shown by the blue line.

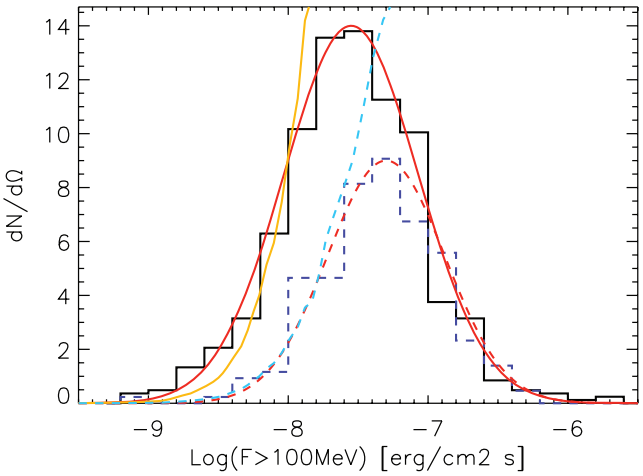

Figure 4. Flux distribution of *Fermi* sources of the 1LAC sample located at high Galactic latitudes ($|b| > 20^\circ$, solid histogram) and located along the Galactic plane ($|b| < 20^\circ$, dashed blue histogram). The two distributions are normalized to the corresponding solid angles. The solid and dotted red lines are two Gaussians fitting the flux distributions. The dashed (cyan) and solid (orange) lines show the detection efficiency (adapted from Abdo et al. 2010c) and scaled by a factor of 3 between the two histograms.

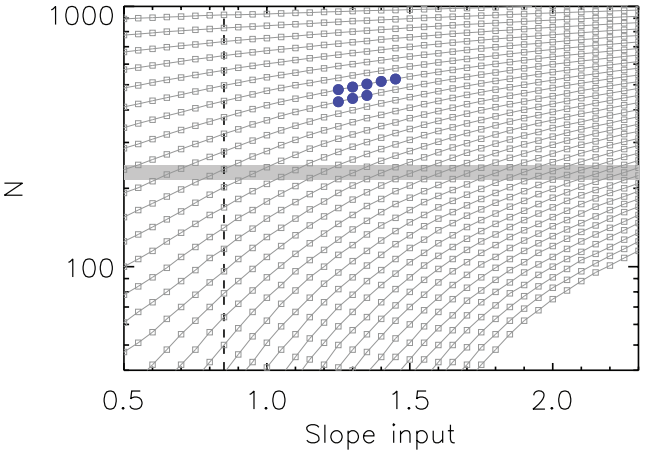

Figure 5. Simulation results. The number of simulated sources (which survive the two instrumental selection effects S1 and S2 described in the text) is plotted against the slope $\hat{\delta}$ of the assumed $\hat{F}_\gamma$–$\hat{F}_\mathrm{r}$ correlation. Each curve represents a set of simulations of the $\hat{F}_\gamma$–$\hat{F}_\mathrm{r}$ correlation with fixed normalization $\hat{K}$ and varying slope $\hat{\delta}$. The open squares are those cases of ($\hat{\delta}$, $\hat{K}$) where more than 68 per cent of the simulations fail to reproduce the observed source distribution of the real sources in the F_γ–F_r plane (i.e. in more than 68 per cent of the simulations, the simulated-source F_γ and F_r distributions have KS probabilities <1 per cent of being consistent with the F_γ and F_γ distributions of the real sources). The acceptable simulations are shown by the filled blue circles. The simulations are performed assuming equation (1) for the γ-ray variability function that, after averaging, results in a very modest flux variability. The shaded region represents the number of real sources (i.e. 230 ± 15) detected by *Fermi* with a radio counterpart which give rise to the observed F_γ–F_r correlation. For reference, the vertical dashed line shows the slope of the observed F_γ–F_r correlation.

simulated sources surviving the S2 selection (hereinafter 'detectable sources') are the red dots in Fig. 3.

Their distributions in the F_γ–F_r plane is compared with the distribution of real sources in the same plane. First, we compare independently the distributions of F_γ and F_r of the detectable and real sources through the KS test and derive the corresponding probabilities $P(\mathrm{KS})_\gamma$ and $P(\mathrm{KS})_\mathrm{r}$. The two histograms (of the detectable and real sources) are shown in the left-hand side and bottom panels of Fig. 3. We consider that the detectable and the real sources have similar distributions in the F_γ–F_r plane when the KS probabilities are both $>10^{-2}$.

Then, for each assumed $\hat{F}_\gamma$–$\hat{F}_\mathrm{r}$ correlation (with fixed slope and normalization, $\hat{\delta}$ and $\hat{K}$, respectively), we repeat the simulation 300 times and count the number of simulations yielding a KS probability >1 per cent that *both* the radio and γ-ray flux distributions of detectable and real sources are drawn from the same parent population.

We consider a set of input parameters ($\hat{\delta}$, $\hat{K}$) acceptable when more than 68 per cent of the 300 simulations had $P(\mathrm{KS})_\gamma$ and $P(\mathrm{KS})_\mathrm{r}$ larger than 1 per cent.

Finally, among the acceptable simulations, we identified those producing a number of detectable sources (red points in Fig. 3) equal to the real one (i.e. 230 ± 15, open blue squares in the example of Fig. 3). In the example shown in Fig. 3, the number of simulated sources detectable by *Fermi* is ∼250. These simulations give us the slope and normalization of the true $\hat{F}_\gamma$–$\hat{F}_\mathrm{r}$ correlation we are seeking.

5 RESULTS

In the following section, we present the results obtained through our simulations under the two possible variability scenarios for the γ-ray flux discussed in Section 3.

5.1 Simulations with the short-term γ-ray variability

In Fig. 5, we show the number of simulated sources detectable by *Fermi* versus the slope $\hat{\delta}$ of the $\hat{F}_\gamma$–$\hat{F}_\mathrm{r}$ correlation. These are the results obtained assuming a short-term variability of the γ-ray flux described in Section 3.2. Each curve represents a different normalization $\hat{K}$ of the $\hat{F}_\gamma$–$\hat{F}_\mathrm{r}$ correlation. The open grey squares in Fig. 5 are those simulations rejected, because the distribution of F_γ and/or F_r of the simulated sources is inconsistent with those of the real sources, that is, $P(\mathrm{KS})_\gamma$ and/or $P(\mathrm{KS})_\mathrm{r} < 10^{-2}$, in more than 68 per cent of the repeated simulations.

Conversely, the filled circles correspond to distributions of simulated sources (i.e. the red points in Fig. 3) in the F_γ–F_r plane consistent with the distribution of the real sources, that is, in more than 68 per cent of the repeated simulations (for each choice of the free parameters $\hat{\delta}$ and $\hat{K}$), $P(\mathrm{KS})_\gamma$ and $P(\mathrm{KS})_\mathrm{r} > 10^{-2}$.

The results shown in Fig. 5 are obtained under the hypothesis that the short time-variability of the γ-ray flux is described by equation (1), implying a very modest variation in the average flux. We note that all the acceptable simulations (filled circles) overpredict the number of sources with respect to the 230 *Fermi*-detected sources with an AT20G counterpart (G10). Therefore, a modest variability in the average γ-ray flux cannot reproduce the number of sources really observed in the F_γ–F_r plane for any assumed true $\hat{F}_\gamma$–$\hat{F}_\mathrm{r}$ correlation.

5.2 Simulations with the long-term γ-ray variability

The next step was to assume a larger variability function for F_γ, that is, a lognormal distribution with $\sigma_\gamma = 0.5$. The results of the simulations under this assumption for the variability of F_γ are shown in Fig. 6 (filled blue circles). In this case, the acceptable $\hat{F}_\gamma$–$\hat{F}_\mathrm{r}$ correlations extend over a wider parameter range of normalization and slope, $\hat{K}$ and $\hat{\delta}$, of the $\hat{F}_\gamma$–$\hat{F}_\mathrm{r}$ correlation with respect to the

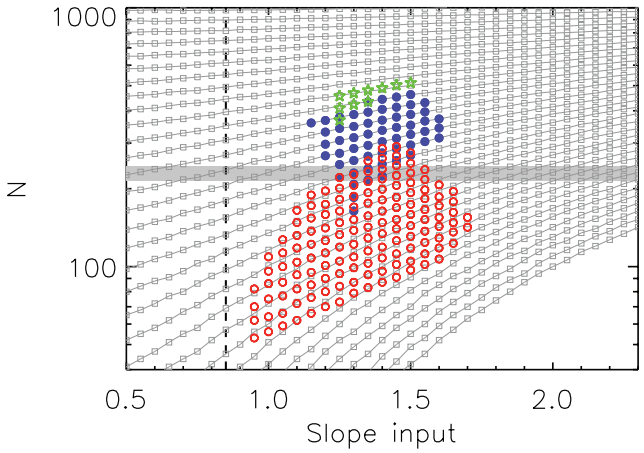

Figure 6. Same as Fig. 5, but with a variability function for the γ-ray flux which is a lognormal with $\sigma_\gamma = 0.5$ (filled blue circles). Also shown are the results assuming a γ-ray lognormal variability function with $\sigma_\gamma = 0.18$ and 0.78 (shown by the open green stars and the open red circles, respectively).

acceptable simulations shown in Fig. 5. This is due to the assumed larger amplitude variability. In this case, there is a set of simulations (those intersecting the horizontal shaded stripe in Fig. 6) that can also reproduce the real number of observed sources. Therefore, the solutions we find in this case correspond to $-8.7 < \hat{K} < -8.3$ and $1.25 < \hat{\delta} < 1.5$.

The results shown in Fig. 5 on the slope and normalization can be understood with the aid of Fig. 3. The distribution of real sources in the F_γ–F_r plane (open blue squares in Fig. 3) is constraining. For instance, for very low normalizations $\hat{K}$ of the $\hat{F}_\gamma$–$\hat{F}_r$ correlation, the number of simulated points surviving the selection effect S2, that is, the red points in Fig. 3, is lower than 230 and their distributions of F_γ and F_r are inconsistent with that of the real sources. This is the case of the simulations below the shaded stripe (representing the number of real sources in the F_γ–F_r plane) in Fig. 5.

However, when a lognormal function is assumed for the variability of F_γ, the spread of the simulated points in F_γ can be larger and, although the detectable sources are much fewer than the real ones, their F_γ and/or F_r distributions can still be consistent with those of the real sources. This explains why there are solutions in Fig. 6 which are acceptable although the number of detectable sources is smaller than that of the real ones.

Although the choice of a lognormal variability function with $\sigma_\gamma = 0.5$ is motivated by the long-term variability of the EGRET sources detected by *Fermi*, we also verified how the solutions of the simulation depend on the choice of σ_γ. In particular, we tested a lognormal variability function with $\sigma_\gamma = 0.18$ and 0.78 corresponding to a linear flux variation by a factor of 1.5 and 6, respectively. The solutions are shown in Fig. 6 by the open star and circles, respectively. We find that $\sigma_\gamma = 0.18$ introduces a too small degree of variability (similar to the variability function of equation 1) and all the solutions overpredict the number of detectable sources with respect to the real number of associations. On the other hand, a larger variability (i.e. $\sigma_\gamma = 0.78$) extends the space of acceptable solutions below those obtained with $\sigma_\gamma = 0.5$. Note that the position of the red open circles and green open stars in Fig. 6 (corresponding to simulations with $\sigma_\gamma = 0.78$ and 0.15, respectively) does not exactly coincide with that of the filled blue circles. This is because the three sets of simulations, shown in Fig. 6, have slightly different normalizations even when the slope is equal. For clarity, in Fig. 6, we draw only the curves (open grey connected squares) corresponding to the simulation with $\sigma_\gamma = 0.5$.

As a caveat we stress that in our simulations, we adopted the *Fermi* sensitivity computed by Abdo et al. (2010c) which assumes a spectral index distribution typical of FSRQs. While it is known that the *Fermi* sensitivity strongly depends on the source spectral index (e.g. Abdo et al. 2010a), it should be noted that our sample of 1FGL–AT20G associations is dominated by FSRQs. For BL Lac objects, the better sensitivity of *Fermi* in detecting these hard sources would imply a lower detection limit (represented by the shaded region S2 in Fig. 1). This would require, in order to reproduce the observed F_γ–F_r correlation, a combination of a slightly smaller normalization and slope of the $\hat{F}_\gamma$–$\hat{F}_r$ correlation possibly coupled with a slightly larger variability of the γ-ray flux. Still the results would be comparable with those derived with the detection sensitivity of FSRQs, since we find that a variability of at least a factor of 3 (i.e. $\sigma = 0.5$) is necessary to reproduce the F_γ–F_r correlation.

5.3 Predicted number of *Fermi* detectable sources

The *Fermi* sensitivity is increasing with the increasing exposure time of its survey. We can use the simulation and the reconstructed $\hat{F}_\gamma$–$\hat{F}_r$ correlation to infer the number of sources that will be detected with a future increase in the survey time which will improve the 11-month *Fermi* survey limit by a factor of 2. We expect that a larger number of detected γ-ray sources will have a counterpart in the AT20G radio survey. By running our simulation with the best correlation found in the previous section, we find that the total number of southern sources present in the AT20G that will be detected by *Fermi* will go from the current 230 to ∼430. This number is in agreement with what expected if the radio $\log N$–$\log S_r$ has slope –3/2 and considering the reconstructed correlation $\hat{F}_\gamma \propto \hat{F}_r^{1.5}$, and implies a γ-ray $\log N$–$\log S_\gamma$ with a slope flatter than Euclidean.

5.4 γ-ray–radio luminosity correlation

The possible correlation between the radio and the γ-ray luminosity has been studied in the past with the aid of EGRET detected sources. Different groups reported a significant correlation between the radio luminosity (at frequencies larger than 1 GHz) and the γ-ray one (e.g. Salamon & Stecker 1996; Fossati et al. 1998) of blazars detected by EGRET. Bloom (2008) found $L_\gamma \propto L_r^{0.77\pm0.03}$ with a sample of 122 sources identified as blazars in the revised EGRET sample. Mucke et al. (1997) argued that the correlation could be due to instrumental biases coupled to the use of average γ-ray fluxes that washes out the considerable variability of blazars at γ-ray wavelengths. None the less, Zhang, Cheng & Fan (2001), through partial correlation analysis, showed that a marginal correlation exists between the radio and the γ-ray luminosity in EGRET blazars, considering the high- and low-state fluxes of EGRET sources nearly simultaneously observed in the radio band. More recently, Pushkarev, Kovalev & Lister (2010) showed that there exists a strong correlation between the γ-ray and the VLBA radio flux on monthly time-scales and that the radio flux lags the γ-ray one by 1–8 months.

Among the 230 AT20G–1LAC associations, there are 144 sources (112 FSRQs, 22 BL Lac objects and 10 'AGNs') with measured redshifts. In Fig. 7, we show them in the γ-ray versus radio luminosity plane. Both luminosities have been K-corrected using the radio and γ-ray spectral index of individual sources. While the γ-ray luminosity is integrated above 100 MeV, the radio one is the νL_ν luminosity

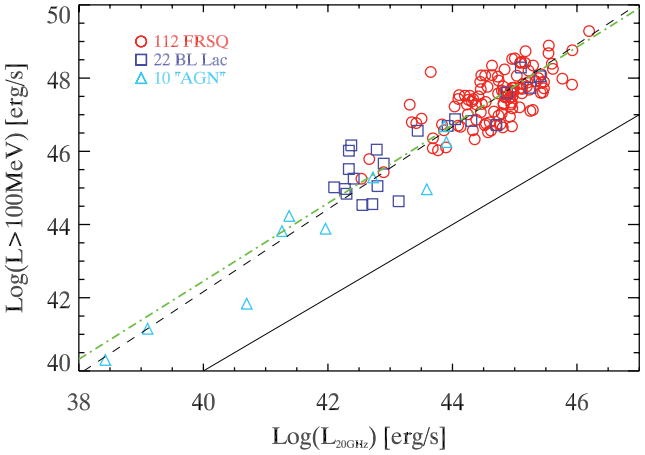

Figure 7. K-corrected γ-ray luminosity (integrated above 100 MeV) versus radio luminosity (νL_ν at 20 GHz) for the 112 FSRQs, 22 BL Lac objects and 10 'AGNs' (different symbols as shown in the legend) of the AT20G–1LAC association sample with measured redshifts. The solid line represents equality. The dashed line is the fit considering all the sources (slope 1.13) and the dot–dashed line is the fit considering only FSRQs and BL Lac objects (slope 1.07).

computed at 20 GHz. FSRQs, BL Lac objects and 'AGNs' are distributed along a linear correlation. Considering only FRSQs and BL Lac objects (circles and squares in Fig. 7), the correlation has a slope 1.07 $\pm$ 0.05 (dot–dashed line in Fig. 7). A somewhat steeper slope 1.13 $\pm$ 0.04 is found if 'AGNs' are also included in the fit (i.e. considering all 144 sources).[2] This value is steeper than that found by Bloom (2008) and also that of the correlations (both for the low/high states and for the average flux case of EGRET blazars) reported by Zhang et al. (2001).

Given the common dependence of the γ-ray and radio luminosity on the redshift z, we should test if the L_γ–L_r correlation is true. Several methods have been applied to investigate this possibility (e.g. Mucke et al. 1997; Zhang et al. 2001; Bloom 2008). We perform a partial correlation analysis by removing the dependence of both L_γ and L_r on the redshift z (e.g. Padovani 1992). We computed the Spearman correlation coefficients and the associated probabilities and then the partial correlation coefficient and the probability of the null hypothesis that the two luminosities are uncorrelated. The chance probability of the partial correlation coefficient is distributed as a t-statistic. All the values of the correlation coefficients and the associated probabilities are reported in Table 1. We note that considering the FSRQs and BL Lac objects together the partial correlation probability of the null hypothesis is 10^{-10}. This result indicates, in agreement with that reported by Bloom (2008), that indeed a strong L_γ–L_r correlation exists in blazars. However, by considering BL Lac objects and AGNs separately, we find a high chance probability of the partial correlation coefficient. This suggests that, although we still have few sources of these classes, their large redshift spread makes the luminosity correlation less statistically significant than for the class of FSRQs.

5.5 Contribution of blazars to the γ-ray background radiation

The existence of a L_γ–L_r correlation and of a corresponding correlation in the observer frame (i.e. the $\hat{F}_\gamma$–$\hat{F}_\mathrm{r}$ correlation found in this paper) could also have some implications for the computation of the contribution of blazars to the extragalactic γ-ray background radiation (EGBR). One method often adopted to this end uses a linear relation between the γ-ray luminosity of blazars and the luminosity at some other wavelength in order to rescale the γ-ray luminosity function through the often better-known luminosity function at the other wavelength (e.g. Salamon & Stecker 1996; Norumoto & Totani 2007). Alternatively, one can construct the γ-ray luminosity function of blazars starting from a catalogue, like the Fermi First Blazar Catalog. The latter method has been recently applied by Abdo et al. (2010c).

Fermi finds (Abdo et al. 2010d) that the EGBR spectrum is consistent with a power law with spectral index 2.41 $\pm$ 0.05 and an integrated (>100 MeV) flux of 1.03×10^{-5} cm^{-2} s^{-1} sr^{-1}, which is softer and less intense with respect to the measurements of EGRET. Note that the above value is not the total background, but the one obtained by subtracting the detected sources. It contains the contribution of undetected sources which have either a flux below the *Fermi* sensitivity threshold (corresponding to the flux of the faintest source detected by *Fermi*) or that are not detected (but with a flux larger than this limit) because of their intrinsic properties (e.g. soft spectrum or position in the sky coincident with regions of high diffuse background level – see Abdo et al. 2010c). Recently, Abdo et al. (2010c) considered the contribution of blazars to the EGBR. They point out that, due to the detection efficiency of *Fermi* (that we also used in this work), there is a substantial fraction of γ-ray sources which are not detected but still have a flux larger than the flux of the faintest source detected by *Fermi*. Therefore, from their count distribution, they estimate that non-detected blazars, but with a flux larger than the faintest detected source limit, should contribute ~16 per cent of the EGBR flux (to which detected *Fermi* sources have been subtracted). By extrapolating the blazars' count distribution to zero flux, this estimate becomes 23 per cent (Abdo et al. 2010c).

We can perform a simple exercise: we assume that all the radio sources in the AT20G survey with flat radio spectrum are candidate blazars emitting in the *Fermi* energy band. Through the $\hat{F}_\gamma$–$\hat{F}_\mathrm{r}$ correlation, we can compute their integrated F_γ that can be compared with the level of the γ-ray background. This estimate should be compared with the EGBR flux including the detected sources, that is, roughly a factor of 1.3 larger than the EGBR flux used in Abdo et al. (2010c) from which the detected sources were removed. The diffuse EGBR we use is adapted from fig. 3 of Abdo et al. (2010d) where the EGBR and the contribution of detected sources are shown separately.

Table 1. Partial correlation analysis of the L_γ–L_r correlation accounting for the common redshift dependence. Each row gives the Spearman correlation coefficients and in the last column is reported the partial correlation coefficient. The probabilities of the correlation coefficient are also given.

Sources	L_γ–L_r	L_γ–z	L_r–z	L_γ–L_r (z)
All (144)	0.8	0.89	0.72	0.5
	10^{-34}	10^{-45}	10^{-25}	10^{-11}
FSRQs (112)	0.66	0.83	0.54	0.44
	10^{-15}	10^{-30}	10^{-10}	10^{-7}
BL Lac objects (22)	0.78	0.90	0.78	0.29
	10^{-5}	10^{-9}	10^{-5}	10^{-1}
AGNs (10)	0.96	0.97	0.94	0.56
	10^{-6}	10^{-6}	10^{-5}	10^{-1}
FSRQs + BL Lac objects (134)	0.76	0.86	0.67	0.5
	10^{-27}	10^{-42}	10^{-18}	10^{-10}

[2] All the fits are performed with the bisector method (e.g. Isobe et al. 1990).

We use the reconstructed $\hat{F}_\gamma$–$\hat{F}_r$ correlation with slope in the range 1.25–1.4 (corresponding to the acceptable solutions in Fig. 6, filled circles) and perform a set of 300 simulations by first assigning to the 3686 flat radio spectrum AT20G sources an $\hat{F}_\gamma$ through this assumed correlation and then assigning an F_γ according to a lognormal γ-ray flux variability with $\sigma_\gamma = 0.5$ (Section 4). For each simulation, we calculate the total γ-ray flux contributed by the flat radio sources. On average, we find that their contribution (according to the assumed correlation slope and normalization) ranges between $\sim$37 $\pm$ 5 and the $\sim$52 $\pm$ 5 per cent (for slopes 1.25 and 1.4, respectively) of the EGBR including the detected sources. This fraction is made by two contributions: the total flux of detected sources (i.e. the 230 AT20G–*Fermi* associations) which can be between 20 and 35 per cent of the EGBR, while the remaining 17 per cent is the contribution of undetected sources belonging to the population of flat radio sources with $F_r \geq 40$ mJy (i.e. in the AT20G survey). Based on model population studies of blazars, Inoue et al. (2009) find that the contribution of blazars to the EGBR (including detected sources) should be 45 per cent (an additional 35 per cent should be due to non-blazar AGNs). This estimate is consistent with the range derived from our analysis. We note that in our estimate we are considering the combined contribution of FRSQs and BL Lac objects, although they have different γ-ray spectral properties (the latter, having a harder spectrum in the *Fermi* band, are very likely dominating the contribution to the EGBR at high energies) and redshift distributions. However, we have used the $\hat{F}_\gamma$–$\hat{F}_r$ correlation for our estimate and we have shown (G10) that both these classes of sources follow a similar correlation between the radio and the γ-ray flux.

5.6 Predictions for the brightest γ-ray blazars

One possible application of the $\hat{F}_\gamma$–$\hat{F}_r$ correlation obtained in this paper is to predict the average γ-ray flux and its maximum value for any given blazar with known radio flux density at 20 GHz. Fig. 8 shows the AT20G–1LAC associations (G10) and the reconstructed correlation (here we have chosen to report the solution with slope

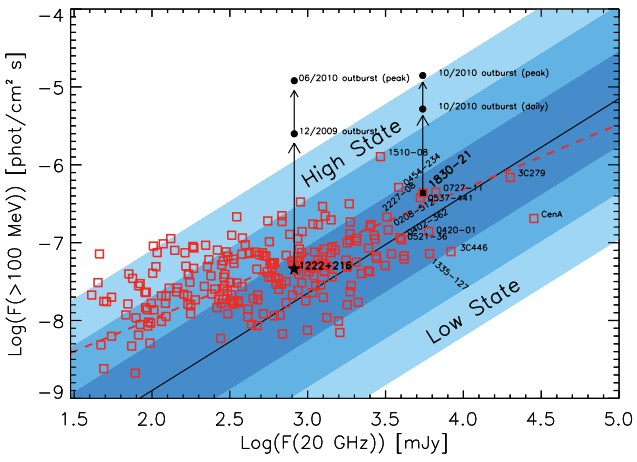

Figure 8. γ-ray flux versus radio flux density of the AT20G–1LAC associations (open red squares). The solid line represents the reconstructed $\hat{F}_\gamma$–$\hat{F}_r$ correlation and its 1, 2 and 3σ_γ scatter (with $\sigma_\gamma = 0.6$) is shown by the shaded regions. The names of the brightest sources are shown. The region above the solid line (with slope 1.25) represents the high state, that is, a source can vary its average F_γ within the shaded regions according to a lognormal probability function with assigned σ. The dashed line is the F_γ–F_r correlation. The outbursts, detected by *Fermi*, of two sources, PKS 1222+216 and PKS 1830−21, are shown.

1.25), and its 1, 2 and 3σ_γ dispersion. The $\hat{F}_\gamma$–$\hat{F}_r$ correlation divides the plane of Fig. 7 into two regions that we label as 'low' and 'high' states. These correspond to those states of the γ-ray flux (1, 2 or 3σ) above or below the average value represented by the $\hat{F}_\gamma$–$\hat{F}_r$ correlation (solid line in Fig. 8). The shaded regions in Fig. 8 show how the average flux (over 11 months as measured by *Fermi* in its survey, which is the one we used to construct the F_γ–F_r correlation) can vary according to a lognormal distribution with $\sigma_\gamma \sim 0.6$.

We have considered the brightest blazars, with F_r at $\sim$20 GHz larger than 3 Jy, distributed in the Southern (i.e. present in the AT20G survey) and Northern hemispheres. For them we can calculate the average $\hat{F}_\gamma$ and the maximum average F_γ they can reach if their long-term variability follows the lognormal distribution found for the sources in common between EGRET and *Fermi*. These values of $\hat{F}_\gamma$ and $F_{\gamma,3\sigma}$ are given in Table 2. Among the sources are 3C 279 and 3C 273 in which the γ-ray flux can be larger than 5×10^{-5} photon cm^{-2} s^{-1} . Furthermore, Tavecchio et al. (2010) showed that in the brightest blazars, a short-term variability (Section 3) can be present and modulate the γ-ray flux by a factor of 3 (or even 10 in the most extreme cases), on top of the long-term variability. Therefore, they could reach even larger fluxes through sporadic flares of emission, like the case of 3C 454.3 last year (Foschini et al. 2010; Bonnoli et al. 2011), increasing their F_γ from the highest average value (i.e. $F_{\gamma,3\sigma}$) still by a factor of a few. Table 2 provides the list of those sources which can be included in long-term multiwavelength monitoring of blazars for the study of their variability and for the characterization of the most-extreme phases of their emission.

An interesting case is represented by 4C+21.35 (PKS 1222+216 at $z = 0.43$). In 2009 April, this source increased its average F_γ flux by a factor of 10 with respect to its average flux of $\sim 4.6 \times 10^{-8}$ photon cm^{-2} s^{-1} measured in the *Fermi* first 6-month survey (Longo et al. 2009). A strong flare was detected by *AGILE*/GRID in 2009 December (Verrecchia et al. 2009) with a flux (integrated above 100 MeV) of 2.5×10^{-6} photon cm^{-2} s^{-1} and confirmed by *Fermi* (with flux 3.4×10^{-6} photon cm^{-2} s^{-1}, Ciprini et al. 2009). In the period 2010 April–May, GeV flares were detected by *Fermi* (Donato et al. 2010) at a flux level of 8×10^{-6} photon cm^{-2} s^{-1}, that is, a factor of about 4 in excess with respect to the average flux of that period and by *AGILE* (Bulgarelli et al. 2010). Very high emission (above 100 GeV) was also found from this source in this period (Mariotti et al. 2010; Neronov et al. 2010). Finally, in 2010 June, *Fermi* recorded a flux of 1.2×10^{-5} photon cm^{-2} s^{-1} (Iafrate et al. 2010) which represents an increase by a factor of 3 with respect to the average flux of the week.

4C+21.35 has a radio flux (at 15 GHz) of about 1 Jy. The $\hat{F}_\gamma$–$\hat{F}_r$ correlation can be used to calculate its average flux level and its average 3σ flux level. These turn out to be $\hat{F}_\gamma = 2.2 \times 10^{-8}$ photon cm^{-2} s^{-1} and $F_{\gamma,3\sigma} = 1.4 \times 10^{-6}$ photon cm^{-2} s^{-1}. We note that the brightest flare of 4C+21.35 detected by *Fermi* in 2010 June has a flux a factor of $\sim$10 larger than the maximum average flux predicted from the $\hat{F}_\gamma$–$\hat{F}_r$ correlation, that is, if the source were 3σ brighter than its average flux as predicted by the correlation.

As already discussed, one possibility is that while the average flux (i.e. the average as measured by *Fermi* in its 11-month survey) is modulated by a long-term variability following a lognormal distribution as found in the case of the EGRET sources detected by *Fermi* (see Section 3); on top of this, there is a much shorter variability (described by equation 1) as found in the brightest blazars (Tavecchio et al. 2010). This short-time-scale variability operates on top of each state of the average γ-ray flux and can boost the

Table 2. Blazars with the highest radio flux density at 20 GHz, that is, $F_r \geq 3$ Jy, distributed in the Southern and Northern hemispheres (top and bottom parts, respectively). For each source are reported its name and the radio flux density [for Southern hemisphere sources, this is extracted from the AT20G survey (Murphy et al. 2010), while for the Northern hemisphere sources, it is taken from the NASA Extragalactic Data base and in most cases it is at 22 GHz]. We also give the average γ-ray flux F_γ calculated from the reconstructed $\hat{F}_\gamma$–$\hat{F}_r$ correlation (i.e. solid line in Fig. 8) and its 3σ highest value corresponding to the highest possible state according to a lognormal variability of the γ-ray flux with $\sigma_\gamma = 0.6$ (shaded region in Fig. 8).

Source	F_r (Jy)	$\hat{F}_\gamma$ (photon cm^{-2} s^{-1})	$F_{\gamma,3\sigma}$ (photon cm^{-2} s^{-1})
3C 279	20.0	9.5e−7	6.0e−5
[HB89] 1921−293	13.8	6.0e−7	3.8e−5
3C 446	8.3	3.2e−7	2.0e−5
PKS 0727−11	6.7	2.4e−7	1.5e−5
PKS 1335−127	6.1	2.1e−7	1.4e−5
PKS 0420−01	6.0	2.1e−7	1.3e−5
PKS 1830−21	5.5	1.9e−7	1.2e−5
PKS 0537−441	5.3	1.8e−7	1.1e−5
PKS 0454−46	4.2	1.3e−7	8.5e−6
CRATES J0609−0615	4.2	1.3e−7	8.5e−6
PKS 0402−362	4.0	1.2e−7	8.0e−6
PKS B0607−157	4.0	1.2e−7	8.0e−6
PKS 0521−36	4.0	1.2e−7	8.0e−6
PKS 0454−234	3.8	1.2e−7	7.5e−6
PKS 1954−388	3.8	1.2e−7	7.5e−6
AP LIB	3.4	1.0e−7	6.5e−6
PKS 0208−512	3.3	1.0e−7	6.3e−6
PKS 2227−08	3.2	9.6e−8	6.0e−6
PKS 0637−75	3.1	9.2e−8	5.8e−6
PKS 1510−08	2.9	8.5e−8	5.3e−6
3C 273	23.8	1.2e−6	7.4e−5
3C 345	12.0	5.0e−7	3.2e−5
3C 454.3	11.0	4.5e−7	2.3e−5
87GB[BWE91] 0059+5808	8.6	3.3e−7	2.1e−5
[HB89] 2145+067	8.5	3.3e−7	2.1e−5
OJ +287	6.0	2.1e−7	1.3e−5
[HB89] 0735+178	5.3	1.8e−7	1.1e−5
[HB89] 2134+004	5.1	1.7e−7	1.1e−5
[HB89] 0923+392	5.0	1.7e−7	1.1e−5
BL Lac	4.5	1.5e−7	9.2e−6
[HB89] 2201+315	4.5	1.5e−7	9.2e−6
4C +50.11	4.2	1.3e−7	8.4e−6
[HB89] 1055+018	4.2	1.3e−7	8.5e−6
[HB89] 1308+326	3.9	1.2e−7	7.6e−6
[HB89] 1611+343	3.6	1.1e−7	6.9e−6
[HB89] 1928+738	3.5	1.1e−7	6.7e−6
LBQS 0106+0119	3.5	1.1e−7	6.8e−6
[HB89] 2005+403	3.4	1.0e−7	6.4e−6
[HB89] 0234+285	3.4	1.0e−7	6.5e−6
[HB89] 0642+449	3.3	1.0e−7	6.4e−6
[HB89] 1749+096	3.3	1.0e−7	6.3e−6

flux still by a factor of 3–10 even when the source has reached its maximum value of the average flux.

In Fig. 8, we show the variations in the γ-ray flux of PKS 1222+216 caught to be in outburst by both *Fermi* and *AGILE* on 2009 December 2009 (Ciprini et al. 2009; Verrecchia et al. 2009) and to reach in 2010 June the flux of 1.2×10^{-5} photon cm^{-2} s^{-1}. We also report the recently detected outburst of PKS 1830−21 (Ciprini et al. 2010), in 2010 October, reaching a daily F_γ of 5.2×10^{-6} photon cm^{-2} s^{-1} with a peak flux of 1.4×10^{-5} photon cm^{-2} s^{-1}.

6 DISCUSSION AND CONCLUSIONS

We studied the F_γ–F_r correlation between the γ-ray (>100 MeV) flux and the radio flux (at 20 GHz) observed in the 230 *Fermi* sources with a counterpart in the AT20G survey (G10). This correlation is biased by the radio flux limit of the AT20G survey and at low γ-ray fluxes by the *Fermi* sensitivity. However, in the F_γ–F_r plane, there are regions (hatched triangles in Fig. 1) where these selection effects are not present and still no source is found. This suggests that the F_γ–F_r correlation is real and yet only 1/15 of the radio sources with flat radio spectra in the AT20G survey have a counterpart in the 11-month *Fermi* survey.

Through numerical simulations, we have recovered the true $\hat{F}_\gamma$–$\hat{F}_r$ correlation that can reproduce the observed F_γ–F_r one. In doing this, we have considered the two main instrumental selection effects (radio flux limit and *Fermi* sensitivity) and tested the possibility that the non-detection of radio sources by *Fermi* could be due to the variability of their emission in the γ-ray energy range. Tavecchio et al. (2010) characterized the variability of 3C 454.3 and PKS 1510−089, two among the brightest blazars detected by *Fermi* (see also Foschini et al. 2010). They found a daily flux distribution which we modelled here through equation (1). However, this 'short' time-scale variability induces a small variation in the γ-ray flux when we average it over 1 yr. A longer time-scale variability is found by comparing, for the sources in common, the fluxes measured by EGRET and, after almost 10 years, by *Fermi*. The ratio of the γ-ray fluxes of the blazars detected by EGRET and *Fermi* has a lognormal distribution with a standard deviation $\sigma_\gamma = 0.5$, and 12 of the 66 blazars detected by EGRET have not been detected by *Fermi*. This suggests that the 'short' time-scale variability is superimposed on a 'decadal' variability and that the latter has a larger relative variation. We considered these two variability patterns in our simulations aimed at recovering the true $\hat{F}_\gamma$–$\hat{F}_r$ correlation of the AT20G–*Fermi* associations.

As shown in Fig. 5, we cannot reproduce the observed F_γ–F_r correlation if we adopt the short time-scale variability (and average the flux over 1 yr). In this case, we overpredict the number of simulated sources detectable by *Fermi* for any combination of the $\hat{F}_\gamma$–$\hat{F}_r$ correlation slope and normalization. Instead, we find (Fig. 6) that the distribution of real sources in the F_γ–F_r plane can be reproduced if the slope of the true $\hat{F}_\gamma$–$\hat{F}_r$ correlation is in the range 1.3–1.5 and if the γ-ray (1-yr-averaged) flux variability is modelled as a lognormal with $\sigma_\gamma \geq 0.5$ (acceptable solutions in Fig. 6 represented by filled and open circles). We also find that a smaller flux variability, also modelled as a lognormal, cannot reproduce the observed F_γ–F_r correlation, similarly to what found by assuming the short time-scale variability pattern of equation (1).

Therefore, we need a 'decadal' γ-ray variability which modulates the 1-yr-averaged γ-ray flux by at least a factor of 3 in order to explain the radio–γ-ray statistical behaviour of blazars. The need to assume such a variability pattern is corroborated by the findings on the ratio of EGRET to *Fermi* flux for the sources in common, although this is based on the EGRET sources which are the most luminous (and maybe the most variable). However, our results show that at least a variability of a factor of 3 in flux is necessary to reproduce the observed radio–γ-ray flux correlation. Recent results, obtained after the 11-month *Fermi* survey, are illuminating: PKS 1222+216 increased its average γ-ray flux by a factor of 300 with respect to its average flux during the first 6-month *Fermi* survey. This implies that the γ-ray flux can vary not only on very short time-scales, but also on longer time-scales and with an amplitude that is larger than what seen in the radio.

For our simulations, we we used the *Fermi* sensitivity computed by Abdo et al. (2010c) which assumes a spectral index distribution typical of FSRQs. Although the *Fermi* sensitivity depends on the source spectral index (e.g. Abdo et al. 2010a), our sample of 1FGL–AT20G associations is dominated by FSRQs. None the less, for BL Lac objects, due to their harder spectrum, a lower *Fermi* detection limit (represented by the shaded region S2 in Fig. 1) should be considered. We remark that based only on the radio data we cannot distinguish, in our simulations, between FSRQs and BL Lac objects among the radio sources with flat radio spectrum but without a γ-ray counterpart. However, if a lower detection sensitivity would be used in our simulations, a combination of a slightly smaller normalization and slope of the $\hat{F}_\gamma$–$\hat{F}_\mathrm{r}$ correlation possibly coupled with a slightly larger variability of the γ-ray flux would be required to reproduce the F_γ–F_r correlation. Still the results would be comparable with those derived with the detection sensitivity of FSRQs.

As a result of the existence of the $\hat{F}_\gamma$–$\hat{F}_\mathrm{r}$ correlation and long-time-scale variability, we also expect that the brightest radio blazars (e.g. with radio flux density $\geq$3 Jy) will always be detected by *Fermi*, since the variability of the γ-ray flux cannot make them much fainter (on average, short-duration events at very low fluxes can occur). Our result also implies that if the average fluxes in the radio and γ-ray bands are correlated, then also a decadal radio flux variation should be expected and with a positive time-delay if the radio-emitting region is larger than the one emitting the γ-rays, and thus is located farther out along the jet.

However, our fluxes are collected at different epochs: the radio data are single snapshots obtained by the AT20G survey in the period 2004–2008, while the *Fermi* fluxes are averages over the 11-month survey between 2008 and 2009. Pushkarev et al. (2010) have shown that there exists a strong correlation between the 15.4-GHz core VLBA flux density and the γ-ray one and that these two fluxes are correlated with a typical delay distributed between 1 and 8 months (in the observer frame) which is interpreted as caused by opacity effects.

This study, on the correlation of *fluxes*, is related to the possibility that there exists a correlation between the γ-ray and the radio *luminosities* in blazars (as found e.g. by Bloom 2008 and discussed in Mucke et al. 1997). Although based on the fraction (144) of the AT20G–*Fermi* associations with measured redshifts, we showed that a strong correlation exists between the radio luminosity and the γ-ray one and that, considering FSRQs and BL Lac objects, it is linear. We also verified, through partial correlation analysis, that this correlation is not due to the common dependence of the luminosities on redshift for FSRQs (null hypothesis probability of the partial correlation, removing the redshift dependence, $P = 10^{-10}$), while only a marginal claim can be made for BL Lac objects alone.

The other main consequence of the existence of a $\hat{F}_\gamma$–$\hat{F}_\mathrm{r}$ correlation in blazars is that it could be used to estimate the contribution of these sources to the γ-ray background (Abdo et al. 2010c). The contribution of blazars can be estimated considering the true $\hat{F}_\gamma$–$\hat{F}_\mathrm{r}$ correlation and the population of radio sources with flat radio spectra (i.e. candidate blazars) in the AT20G survey. We estimate that the blazar contribution to the extragalactic diffuse background is between 37 and 52 per cent (according to the parameters of the assumed $\hat{F}_\gamma$–$\hat{F}_\mathrm{r}$ correlation) of which 17 per cent is the contribution from non-detected sources. Considering that our estimates are based on a flux-limited sample of radio sources (i.e. those with 20-GHz flux larger than 40 mJy), we should expect that if the radio flux limit is further decreased, the number of sources should increase. While detailed predictions depend on the still poorly known $\log N$–$\log S$ of radio sources at very low flux levels, we should expect that the contribution of blazars to the EGRB can even be larger than our present estimates based on a radio-flux-limited sample.

ACKNOWLEDGMENTS

We thank the referee for useful comments and suggestions. This work was partly financially supported by a 2007 COFIN-MIUR grant and ASI I/088/06/0 grant.

REFERENCES

Abdo A. A. et al., 2009a, ApJ, 700, 597
Abdo A. A. et al., 2009b, ApJ, 707, L142
Abdo A. A. et al., 2010a, ApJ, 715, 429
Abdo A. A. et al., 2010b, ApJ, 709, L152
Abdo A. A. et al., 2010c, ApJ, 720, 435
Abdo A. A. et al., 2010d, Phys. Rev., 104, 101101
Abdo A. A. et al., 2010e, ApJ, submitted
Abdo A. A. et al., 2010f, ApJ, 719, 1433
Abdo A. A. et al., 2010g, ApJ, 716, 30
Abdo A. A. et al., 2010h, ApJS, 188, 405
Atwood W. B. et al., 2009, ApJ, 697, 1071
Bloom S. D., 2008, ApJ, 136, 1533
Bonnoli G., Ghisellini G., Foschini L., Tavecchio F., Ghirlanda G., 2011, MNRAS, 410, 368
Bulgarelli et al., 2010, The Astronomer's Telegram, #2641
Ciprini S. et al., 2009, The Astronomer's Telegram, #2349
Ciprini S. et al., 2010, The Astronomer's Telegram, #2943
Donato D. et al., 2010, The Astronomer's Telegram, #2584
Foschini L., Tagliaferri G., Ghisellini G., Ghirlanda G., Tavecchio F., Bonnoli G., 2010, MNRAS, 408, 448
Fossati G., Maraschi L., Celotti A., Comastri A., Ghisellini G., 1998, MNRAS, 299, 433
Ghirlanda G., Ghisellini G., Tavecchio F., Foschini L., 2010, MNRAS, 407, 791
Ghisellini G., Celotti A., Fossati G., Maraschi L., Comastri A., 1998, MNRAS, 301, 451
Giroletti M. et al., 2010, in Proc. Fermi Symp., preprint (arXiv:1001.5123)
Gliozzi M., Foschini L., Sambruna R. M., Tavecchio F., 2008, A&A, 478, 723
Hartman R. C. et al., 1999, ApJS, 123, 79
Iafrate G. et al., 2010, The Astronomer's Telegram, #2687
Inoue Y. et al., 2009, in Proc. Fermi Symp., preprint (arXiv:1001.0103)
Isobe T., Feigelson E. D., Akritas M G., Babu G. J., 1990, ApJ, 364, 104
Kovalev Y. Y., 2009, ApJ, 707, L56
Kovalev Y. Y. et al., 2009, ApJ, 696, L17
Lenc E., Tingay S. J., 2009, AJ, 137, 537
Longo F. et al., 2009, The Astronomer's Telegram, #2021
Mahony E. K., Sadler E. M., Murphy T., Ekers R. D., Edwards P. G., Massardi M., 2010, ApJ, 718, 587
Mariotti M. et al., 2010, The Astronomer's Telegram, #2684
Mucke A. et al., 1997, A&A, 320, 33
Murphy T. et al., 2010, MNRAS, 402, 2403
Neronov D. et al., 2010, The Astronomer's Telegram, #2617
Norumoto T., Totani T., 2007, Ap&SS, 309, 73
Padovani P., 1992, A&A, 256, 399
Pushkarev A. B., Kovalev Y. Y., Lister M. L., 2010, ApJ, 722, L7
Salamon M. H., Stecker F. W., 1996, ApJ, 430, 21
Stecker F. W., Salamon M. H., Malkan M. A., 1993, ApJ, 410, L71
Tavecchio F., Ghisellini G., Ghirlanda G., Foschini L., Maraschi L., 2010, MNRAS, 401, 1570
Taylor G. B. et al., 2007, ApJ, 671, 1355
Verrecchia F. et al., 2009, The Astronomer's Telegram, #2348
Zhang L., Cheng K. S., Fan H., 2001, PASJ, 53, 207

This paper has been typeset from a TEX/LATEX file prepared by the author.